



Combined effects of temperature and axial pressure on dynamic mechanical properties of granite

Tu-bing YIN, Rong-hua SHU, Xi-bing LI, Pin WANG, Long-jun DONG

School of Resources and Safety Engineering, Central South University, Changsha 410083, China

Received 30 August 2015; accepted 6 May 2016

Abstract: In order to get the dynamic mechanical properties of deep rock mass suffered both high temperature and high pressure, impact loading experiments on granite subjected to temperature and axial pressure were carried out. Furthermore, the internal structure characteristics of granite under different temperatures were observed by scanning electron microscopy (SEM). The results show that the longitudinal wave velocity assumes a downward trend which shows a rapid drop before falling slowly as the temperature increases. The uniaxial compressive strength of the specimen decreases significantly at temperatures of 25–100 °C compared to that at temperatures of 100–300 °C. The peak strain rises rapidly before the dividing point of 100 °C, but increases slowly after the dividing point. The internal structure of the rock changes substantially as the temperature increases, such as the extension and transfixion of primary and newborn cracks. In addition, the thermal damage under axial pressure is greater than that described by the longitudinal wave velocity and the phenomenon shows obviously when the temperature increases.

Key words: rock dynamics; split Hopkinson pressure bar; temperature pressure coupling; dynamic mechanical properties

1 Introduction

It is a new challenge for rock mechanics to deal with rock engineering problems at high temperature and high geostress with the development of deep mining. Meanwhile, most rock masses in drilling and blasting undergo dynamic load. In order to ensure safety and efficiency of mining, the above-mentioned rock engineering problems should be solved. All this time, lots of researchers have devoted themselves to study rock mechanical properties under different conditions by various of means. LI et al [1,2] presented a constitutive model of rock under static–dynamic coupling loading and discussed the dynamic problems in deep exploitation of hard rock metal mines. HONG et al [3] analyzed the stress uniformity process in specimens under different loading conditions of rectangular and half-sine input waves. DU et al [4] carried out true triaxial unloading compressive test to study the failure properties of rocks. Using Random Forest, DONG et al [5] predicted the rockburst classification. YIN et al [6] studied the failure

characteristics of high stress rock induced by impact disturbance under confining pressure unloading. In recent years, it has been recognized that temperature is one of the vital factors influencing the mechanical behavior of rock. Temperature plays a significant role in many engineering practices, such as the disposal of highly radioactive nuclear waste, the underground storage and mining of petroleum and natural gas, the development and utilization of geothermal resources, and the post-disaster reconstruction of underground rocks engineering. There are some situations deserve to be mentioned. In Dongguashan Copper Mine of China, the temperature is 40 °C in the depth of 1100 m. And in a gold mine of India, the temperature reaches 69 °C in the depth of 3000 m. What is more, a mine of Japan has exploited a high temperature ore body, where the temperature reaches 100 °C. It is to say that temperature is one of the factors that should be considered in the deep mining. But, all the above researches did not consider the factor of temperature. Since the problem of high temperature was noted and valued, many authors have researched the effect of temperature on the physical and

Foundation item: Project (51304241) supported by the Youth Project of National Natural Science Foundation of China; Project (2014M552164) supported by Chinese Postdoctoral Science Foundation; Project (20130162120015) supported by the Specialized Research Fund for the Doctoral Program of Higher Education of China

Corresponding author: Tu-bing YIN; Tel: +86-18684770361; E-mail: tubing_yin@mail.csu.edu.cn
DOI: 10.1016/S1003-6326(16)64337-6

mechanical properties of various rocks. Some of them discussed the physical and mechanical properties of rocks after high temperature treatment [7–10], and others researched the mechanical properties of rocks under high temperatures [11–14]. The literature indicates that the longitudinal wave velocity of rocks decreases accordingly when the temperature rises. The static and dynamic compressive strengths assume different degrees of variation as the temperature increases. The changes in mineral particles and components of high temperature rocks are significant reasons leading to the changes of their static and dynamic mechanical characteristics. ZHAO et al [15] performed experiments on borehole deformation and instability, and discovered that when the hydrostatic pressure was lower than 100 MPa and the temperature was below 400 °C, the deformation of specimens followed the generalized Kelvin model. LIU and XU [16] carried out a dynamic mechanical experiment on marble. The results indicated that when the temperature reached 1000 °C, the fragments were powder and uniform particles. FUNATSU et al [17] investigated the effects of increasing temperature and confining pressure on the fracture toughness of clay-bearing rock. The investigation showed that the fracture toughness of Kimachi sandstone did not vary significantly as the temperature rose to 125 °C, but it increased at temperatures above 125 °C.

However, many engineering practices mentioned above are related to high temperature, high pressure and dynamic disturbance simultaneously, such as rock bursting in deep mining, drilling and blasting. Due to the differences of geological structure, hydrology and burial depth, the physical and mechanical properties of rocks present regional differences. The physical and mechanical properties of rocks, even if in the same place, may be different. In particular, deep rock mass suffers high temperature and high ground stress at the same time, so the properties of which are likely to change when it undergoes dynamic disturbance. How will the properties of rocks be under that case? They are unknown. In addition, all the above-mentioned research achievements barely address that case and only a few studies have involved the analysis of thermal damage. Consequently, research on the physical and mechanical properties of rock under high temperature, axial pressure and impact loading is extremely urgent. In order to solve the complicated problem, the impact loading experiment of rock under high temperature and pressure could be carried out.

By using the SHPB system with a heating device, the impact loading experiments on granite under high temperature and axial pressure were carried out, and the relationships among peak stress, peak strain, thermal damage and temperature were analyzed.

2 Experimental

2.1 Sample preparation

The rock samples, which were chosen from the same granite block from a quarry in Changsha, China, were processed into cylindrical specimens of $d50 \text{ mm} \times 25 \text{ mm}$ by cutting and polishing. In particular, to ensure the parallelism and flatness, both ends of the samples were polished. The precision control of the specimens was exercised in accordance with the standard requirements of the International Society of Rock Mechanics (ISRM) [18], with the parallelism controlled within $\pm 0.05 \text{ mm}$ and surface flatness within $\pm 0.02 \text{ mm}$. Samples of similar wave velocity were selected by wave velocity determination. The rock samples were mainly composed of plagioclase, quartz, hornblende, biotite, potassium feldspar and a few of other compositions. The main compositions and basic parameters of the samples are listed in Tables 1 and 2, respectively.

Table 1 Main constituents of granite (mass fraction, %)

Plagioclase	Quartz	Hornblende	Biotite	Potassium feldspar	Others
40	19	14	16	6	5

Table 2 Basic parameters of granite samples

Parameter	Value
Average diameter/mm	49.5
Average length/mm	25.5
Average quality/g	127.37
Average density/($\text{kg} \cdot \text{m}^{-3}$)	2596.84
Uniaxial compressive strength/MPa	220
Elastic modulus/GPa	44.50
Wave velocity/($\text{m} \cdot \text{s}^{-1}$)	4160

2.2 Test equipment

The split Hopkinson pressure bar (SHPB) experimental system with a heating device used here is shown in Fig. 1. It mainly consists of a spindle punch, an emission cavity, a gas gun, an incident bar, a transmission bar, an absorbing bar, a data-processing device, a signal recording device, an axial pressure loading device and temperature–pressure coupling device. The bar is made of high strength alloy, with a diameter of 50 mm, an incident bar of 2000 mm, a transmission bar of 1500 mm, an absorbing bar of 500 mm, an ultimate strength of 800 MPa, a wave velocity of 5400 m/s and a density of 7810 kg/m^3 . Strain gauges were fixed on the incident bar and transmission bar respectively and the spindle punch was to guarantee a stable strain rate of the produced half sinusoidal stress

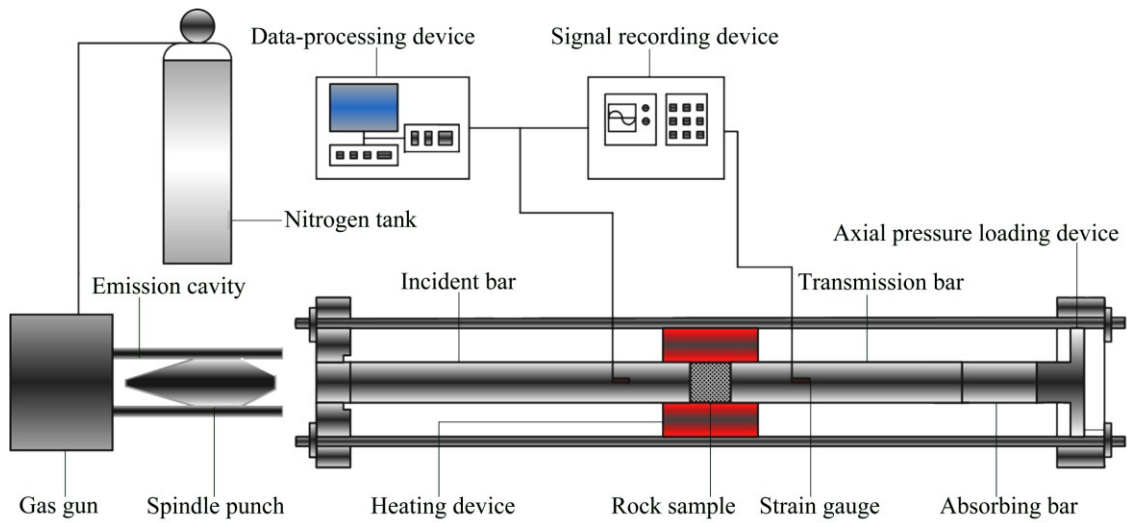


Fig. 1 Split Hopkinson pressure bar (SHPB) system with heating device

wave. The typical stability strain rate of half sinusoidal stress wave is given in Fig. 2.

The temperature–pressure coupling device is shown schematically in Fig. 3. It is primarily composed of heat shell, hearth, heating elements, insulation bin gate and stent. For the heat shell, the material is stainless steel, the diameter is 100 mm, the length is 150 mm and the shape is cylindrical. The hearth is made of carborundum for fireproof purpose. High temperature resistance wire of the type of OCr27Al7Mo2 is used for the heating elements. The insulating layer between the heat shell and hearth is composed of insulating material and aluminum foam brick. The device, which can not only ensure rock samples on the heat source, but also guarantee the precise alignment of the incident bar, rock sample and transmission bar, as well as avoid crushed rock blocks from breaking the heating bonnet, includes a heating cabinet and a temperature controller. The auxiliary heating device of the type SX–4–10, with a rated power of 4 kW and a highest design temperature of 1050 °C

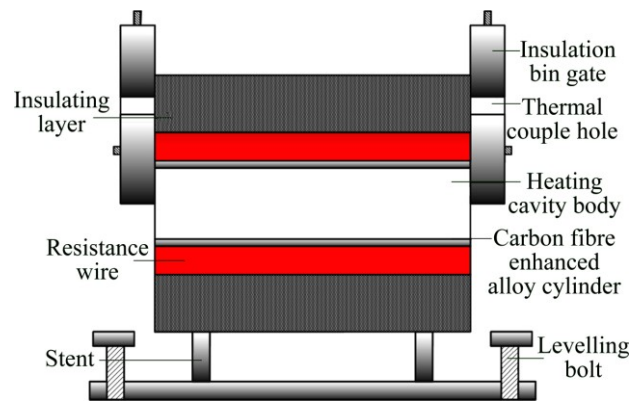


Fig. 3 Internal structure of temperature–pressure coupling device

mainly contains a high temperature furnace and temperature controller. The scanning equipment is an electron microscope. Wave velocity determination is conducted using a rock and soil engineering quality detector which consists of an ultrasonic emission and receiving transducer.

The stress, strain and strain rate of the samples can be calculated by the following formulas:

$$\sigma(t) = \frac{A_0}{2A_s} E(\varepsilon_I + \varepsilon_R + \varepsilon_T) \tag{1}$$

$$\varepsilon(t) = \frac{C_0}{L_s} \int_0^t (\varepsilon_I - \varepsilon_R - \varepsilon_T) \tag{2}$$

$$\dot{\varepsilon}(t) = \frac{C_0}{L_s} (\varepsilon_I - \varepsilon_R - \varepsilon_T) \tag{3}$$

where $\sigma(t)$, $\varepsilon(t)$ and $\dot{\varepsilon}(t)$ stand for stress, strain and strain rate, respectively; C_0 is the wave velocity of the pressure bar and L_s is the length of the pressure bar; A_0 and A_s are the cross-sectional areas of the sample and

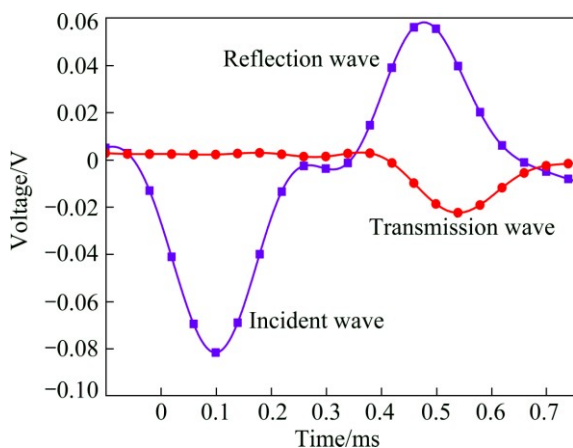


Fig. 2 Typical signal of blast wave

pressure bar, respectively; ε_I , ε_R and ε_T are the incident strain, the reflection strain and the transmission strain, respectively.

2.3 Test procedure

The test temperature is classified into 5 groups: 25, 50, 100, 200 and 300 °C. Each group is equipped with no less than 3 specimens and the axial pressure is 20 MPa. The target temperature with a heating rate of 3 °C/min, once reached, is kept constant for 2 h in order to ensure uniform heating of the samples. Then, the wave velocity of the specimens is measured by using a rock and soil engineering quality detector of type CE9201 no less than three times. After that, the incident bar and transmission bar are pushed into the heating cavity body after the sample is put into the temperature–pressure coupling device. Then, the insulation bin gate is closed after ensuring the fine alignment of the sample and bar. Upon the former step, the axial pressure exerted is 20 MPa with a constant speed and the device is opened to heat the rock sample for 3 min in order to remedy the heat loss. The same air pressure is used to ensure a similar

impact load in each test. Finally, the stress and strain can be calculated from the data recorded by the strain gauges. In addition, the internal structure of the rock specimens can be observed by scanning the fragment using an electron microscope of the type FEI Quanta–200.

3 Results

The test results show certain discreteness due to sample differences and experimental error. But, the figures can generally indicate the correlation between rock parameters and temperature. The failure process consists of the compaction phase, the linear elastic stage, the weakening stage and the failure stage. The uniaxial compressive strength of rock under the axial pressure of 20 MPa is less than that without axial pressure, resulting from the debilitation of the axial pressure on the rock's internal structure. The former is 206.41 MPa and the latter is 220 MPa.

The test data, as listed in Table 3, are given to two decimal places.

The typical stress–strain curve and the stress

Table 3 Summary of parameters of experimental samples

Temperature/ °C	Sample No.	Length/ mm	Diameter/ mm	Mass/ g	Density/ ($\text{kg}\cdot\text{m}^{-3}$)	Peak stress/MPa	Peak strain	Elastic modulus/GPa	Longitudinal wave velocity/ ($\text{m}\cdot\text{s}^{-1}$)
25	1-1	25.58	49.22	129.13	2654.45	201.97	0.00425	44.40	3996.88
	1-2	25.72	49.20	129.68	2653.40	211.95	0.00421	44.76	4386.67
	1-3	26.48	50.34	132.91	2523.15	192.53	0.00426	44.67	4503.17
	1-4	26.76	49.20	134.54	2645.85	203.69	0.00432	43.80	3878.26
	1-5	25.72	49.24	129.12	2637.65	221.90	0.00416	42.60	4018.75
50	2-1	24.44	49.20	122.94	2647.23	175.20	0.00429	40.67	3847.95
	2-2	26.50	49.20	133.47	2650.56	182.02	0.00440	43.26	4010.00
	2-3	26.56	50.80	133.88	2488.23	191.61	0.00430	41.69	4150.00
	2-4	26.00	49.20	130.60	2643.44	171.45	0.00392	41.45	3661.97
	2-5	25.50	49.20	128.65	2655.03	196.30	0.00447	42.26	3695.65
100	3-1	25.10	49.20	131.41	2755.21	155.01	0.00452	36.75	3019.23
	3-2	25.80	49.10	125.87	2577.92	143.67	0.00445	37.62	3154.55
	3-3	25.20	50.20	130.60	2619.78	150.60	0.00460	35.36	3389.66
	3-4	25.96	50.50	140.86	2710.38	153.21	0.00456	33.52	3483.64
	3-5	24.90	50.00	115.21	2357.66	149.12	0.00450	32.72	3204.55
200	4-1	25.10	49.20	121.28	2542.82	130.98	0.00480	29.96	3083.33
	4-2	24.24	49.20	121.98	2648.23	152.08	0.00470	29.64	2723.60
	4-3	25.38	49.50	129.42	2651.12	130.48	0.00465	28.49	2638.00
	4-4	25.50	49.70	128.48	2598.44	142.69	0.00475	25.53	2944.23
	4-5	24.90	49.80	120.03	2476.07	126.61	0.00471	27.46	2569.89
300	5-1	25.24	49.50	127.40	2624.22	124.95	0.00476	24.56	3040.96
	5-2	24.74	49.30	124.98	2647.75	119.48	0.00471	27.25	2444.78
	5-3	25.52	49.50	123.13	2508.44	139.26	0.00482	25.52	2919.05
	5-4	26.44	49.70	127.98	2496.31	133.77	0.00474	27.08	2540.74
	5-5	25.24	49.50	121.74	2507.63	139.27	0.00476	29.52	2786.21

verification are shown in Figs. 4 and 5, respectively. As seen from Fig. 4, although there are some discrepancies in the stress verification, it conforms to the requirements of the impact tests.

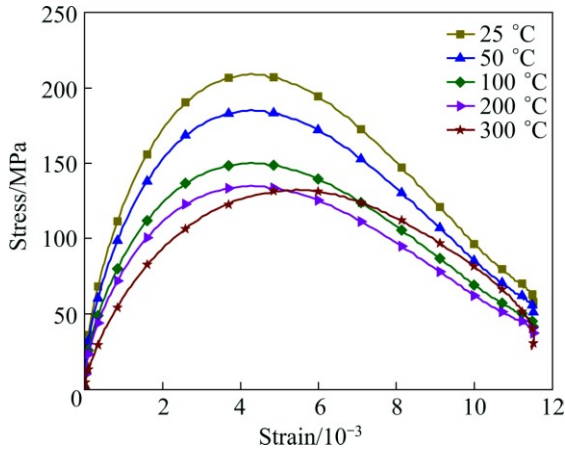


Fig. 4 Typical curves of dynamic stress–strain of sample

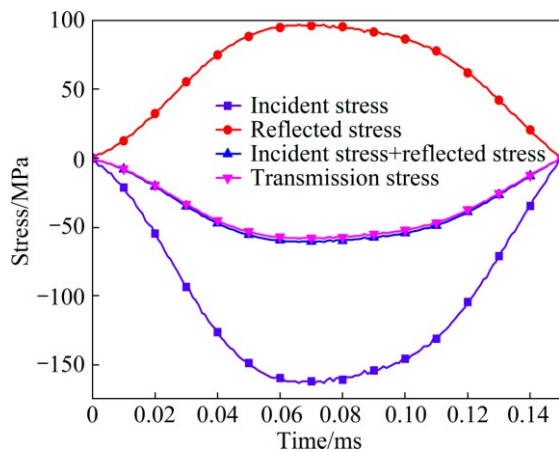


Fig. 5 Stress verification of typical sample

3.1 Temperature effect of peak stress under axial pressure

A concept called relative growth (reduction) is introduced here: the ratio of a rock parameter’s discrepancy at every temperature stage to the corresponding parameter at 25 °C, which can be calculated by

$$B = \left| \frac{A_{T1} - A_{T2}}{A_T} \right| \times 100\% \quad (4)$$

where B and A_T stand for the relative growth (reduction) and the amplitude of every parameter at room temperature, respectively; A_{T1} and A_{T2} are the amplitudes of temperatures T_1 and T_2 , respectively.

Figure 6 shows the correlations between the peak stress of rock specimens and temperature under an axial pressure of 20 MPa. It can be seen that the peak stress has a declining trend. The peak stress is approximately

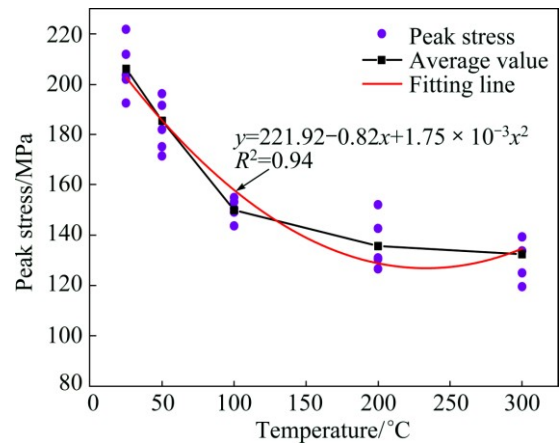


Fig. 6 Correlation between peak stress and temperature of rock under axial pressure of 20 MPa

linear ranging from 25 to 100 °C. The uniaxial compressive strength of the rock decreases from 206.41 to 150.32 MPa and the relative amplitude reduction is as large as 27.17%. There are two main reasons for the changes in the peak stress of the rock. Firstly, the free water evaporates drastically and the density decreases gradually with the increase of temperature. Secondly, the axial pressure inhibits the cracks to expand. In detail, from room temperature to 100 °C, the evaporation of free water leads to the increase of cracks and pores, and the axial pressure causes the weak cracks and pores to close at the same time, but the decreasing rate of cracks and pores is less than the increasing rate. Thus, the porosity increases, the density decreases, and then, the uniaxial compressive strength decreases accordingly. Because of the existence of cracks in the rock, high temperature leads to further expansion of cracks and creation of fissures, and thus the decrease of the peak stress from 150.32 MPa at 100 °C to 136.57 MPa at 200 °C. However, the effect of axial pressure becomes more obvious with the increase of weak cracks and pores, namely, more and more weak cracks and pores close, so, the structure of rock is improved to some extent. In the same time, it is worth noting that the axial pressure inhibits the cracks to expand and the number of cracks also reduces because the mineral compositions expand. But, in general, the porosity shows a decreasing trend. Hence, the relative amplitude reduction at temperatures between 100 and 200 °C is less than that between 25 and 100 °C, which is 6.67%. The peak stress reduces by 5.32 MPa and the relative amplitude reduction is 2.58% when the temperature reaches 300 °C, which are small compared with those at the temperature of 200 °C. The reasons are as follows: before 200 °C, rock sample has already suffered certain damage. When temperature continues to increase, reaching 300 °C, the separation of combined water and the expansion of rock compositions

cause the uniaxial compressive strength to decrease sequentially. And the effect of axial pressure is more obvious compared with that of rock at the temperature of 200 °C. Therefore, the decrease of porosity is lower than the former one and the relative amplitude reduction is smaller than that of rock under temperatures between 100 and 200 °C. By using quadratic function, the relationship between peak stress and temperature is obtained:

$$\sigma = 221.92 - 0.82T + 1.75 \times 10^{-3}T^2 \quad (5)$$

3.2 Temperature effect of peak strain under axial pressure

The peak strain of granite under an axial pressure of 20 MPa shows a non-linear increasing trend with increasing temperature, as seen in Fig. 7. The peak strain ranges from 4.25×10^{-3} to 4.55×10^{-3} under temperatures from 25 up to 100 °C, and the relative amplitude growth is 7.1%. However, when the temperature rises from 100 to 200 °C, the relative amplitude growth is only 4.5%, which is not obvious; and the peak strain changes from 4.55×10^{-3} to 4.74×10^{-3} . As the temperature continues to increase, reaching 300 °C, the peak strain becomes 4.77×10^{-3} and the relative amplitude growth is only 0.71%. To sum up, when temperature increases, the structure of rock suffers a great change, such as the evaporation of free water, the increase of newborn cracks and the decrease of primary cracks. The axial pressure inhibits the primary cracks to expand, even make the primary cracks closed when temperature continues to reach higher. In addition, to some degree, the expansion of mineral compositions causes the primary cracks to close when temperature is high. However, the thermal stress comes out more obviously when temperature is high, thus the number of cracks also shows an increasing trend. As a result, the peak strain increases as temperature increases. The changing trend is not linear because of the difference of the main influencing factors

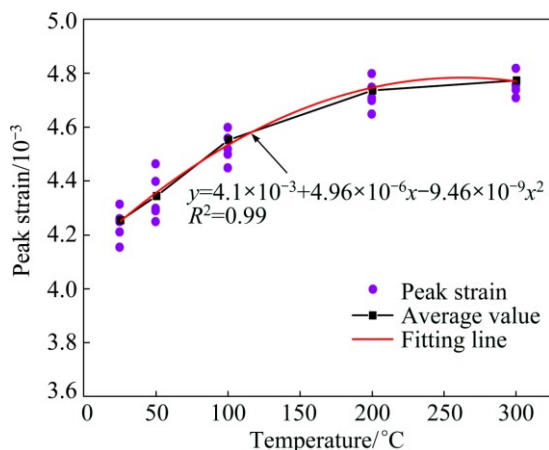


Fig. 7 Correlation between peak strain and temperature of granite under axial pressure of 20 MPa

at each temperature stage. Below 200 °C, owing to the increase of cracks, the porosity increases accordingly, hence, the anti-distortion capacity decreases. Although the axial pressure and the expansion of mineral compositions both inhibit cracks to increase, they are not obvious compared to that above 200 °C. Consequently, the peak strain increases with a nonlinear trend. And the following function could describe the change law of peak strain with the rising temperature.

$$\varepsilon = 4.1 \times 10^{-3} + 4.96 \times 10^{-6}T - 9.46 \times 10^{-9}T^2 \quad (6)$$

3.3 Temperature effect of longitudinal wave velocity

The correlation between the longitudinal wave velocity and temperature of granite is described in Fig. 8. In general, the longitudinal wave velocity presents a declining trend with the increase in temperature. At temperatures from 25 to 50 °C, the longitudinal wave velocity drops from 4156.75 to 3873.11 m/s and the relative amplitude reduction is 6.82%. When heated up to 100 °C, the longitudinal wave velocity drops to 3250.32 m/s, and the relative amplitude reduction is 14.98%. Compared with the former temperature stage, the changes of longitudinal wave velocity and relative amplitude reduction are greater at temperatures from 50 to 100 °C. The reasons can be stated as follows. Firstly, the propagation velocity of ultrasonic waves is obviously higher in liquids and solids than in gas. The pore volume will increase with increasing temperature, which prevents the longitudinal wave velocity from propagating. Secondly, the free water evaporates fully at temperatures between 50 and 100 °C, and the primary cracks extend at the same time. When the temperature rises to 200 °C, the amplitude declines slowly, drops to 458.51 m/s, and the relative amplitude reduction is 11.03%. The main cause is that when the temperature increases, the mineral compositions expand and the number of cracks reduces accordingly. At the temperature of 300 °C, the changes slow down, the relative amplitude reduction is about

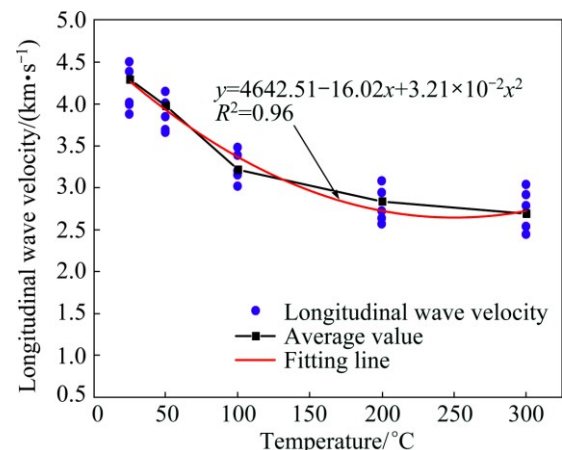


Fig. 8 Correlation between longitudinal wave velocity and temperature of granite

1.09% and the amplitude ranges from only 2791.81 to 2746.35 m/s. This is because the variation of the rock's structure is complete at the previous temperature stage and the number of newborn cracks also reduces relatively. Here gives the function which could describe the relationship between longitudinal wave velocity (v) and temperature.

$$v=4642.51-16.02T+3.21\times 10^{-2}T^2 \quad (7)$$

3.4 Dynamic damage

The dynamic damage of the rock is caused by dynamic disturbance, such as vibration, impact and explosion. Micro-crack initiation, expansion and transfixion lead to the accumulation of damage, causing the inner structure of the rock to show certain changes while the mechanical properties weaken gradually. As is known, impact load occurs commonly in engineering practice, especially in deep rock mass. Therefore, study of the dynamic damage of rock can not only identify the dynamic mechanical properties but also is meaningful for engineering practice. Since the dynamic damage of the rock can be described by various parameters such as the elasticity modulus and wave velocity, the elasticity modulus and longitudinal wave velocity are used to describe this damage.

The elasticity modulus usually contains an initial elastic modulus, tangential elastic modulus and secant elastic modulus. Because of the small fluctuation in the linear elastic stage of the stress–strain curve, the slope of the secant in the linear elastic stage of the stress–strain curve is used to describe the damage, which can be obtained by

$$E = \frac{\sigma_2 - \sigma_1}{\varepsilon_2 - \varepsilon_1} \quad (8)$$

where E , σ_1 and σ_2 stand for the elastic modulus, the initial and terminal stress in the linear elastic stage, respectively, ε_1 is the initial strain in linear elastic stage and ε_2 is the terminal strain in the linear elastic stage.

According to the slope of the secant in the linear elastic stage of the stress–strain curve, the relationship between the elastic modulus and temperature under axial pressure is shown in Fig. 9. Also, the elastic modulus is related to the wave velocity, as shown in the equation:

$$E = \frac{(1 + \mu)(1 - 2\mu)}{1 - \mu} \rho v^2 \quad (9)$$

where E and μ stand for the elastic modulus and Poisson ratio, respectively; ρ is the density and v is the longitudinal wave velocity.

There are some scatters in the elastic modulus curve obtained from the slope of the secant in the linear elastic stage of the stress–strain curve, but the general change varies little. On the whole, the change rule between the

elastic modulus and temperature, which is similar to that between the longitudinal wave velocity and temperature, shows a roughly declining trend.

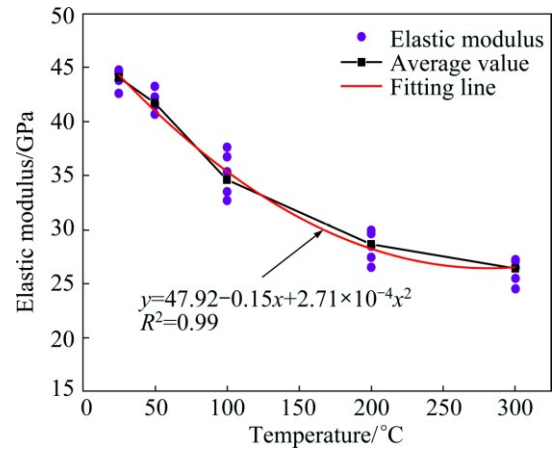


Fig. 9 Correlation between elastic modulus and temperature under axial pressure of 20 MPa

The elastic modulus and longitudinal wave velocity are used to represent the thermal damage respectively, as shown in Eqs. (10) and (11) [19,20]:

$$D_1(T) = 1 - \frac{E_T}{E_0} \quad (10)$$

$$D_2(T) = 1 - \frac{v_T^2}{v_0^2} \quad (11)$$

where $D_1(T)$ and $D_2(T)$ stand for thermal damage; E_T is the dynamic elastic modulus under an axial pressure of 20 MPa at temperature T and E_0 is the dynamic elastic modulus under an axial pressure of 20 MPa at room temperature; v_T is the longitudinal wave velocity at temperature T and v_0 is the longitudinal wave velocity at room temperature.

By using quadratic function, the relationship between temperature and dynamic elastic modulus is obtained.

$$E=47.92-0.15T+2.71\times 10^{-4}T^2 \quad (12)$$

The data on the rock damage under high temperatures are shown in Table 4.

Table 4 Relationship between damage and temperature

Temperature, $T/^\circ\text{C}$	Dynamic thermal damage under axial pressure of 20 MPa, $D_1(T)$	Thermal damage, $D_2(T)$
25	0	0
50	0.09	0.07
100	0.27	0.25
200	0.35	0.34
300	0.4	0.35

According to Table 4, the non-linear relationship between rock damage and temperature is fitted, as seen in Fig. 10. The fitting non-linear functions are shown in Eqs. (13) and (14), respectively:

$$D_1(T)=0.1678\ln T-0.5412 \quad (13)$$

$$D_2(T)=0.1546\ln T-0.5011 \quad (14)$$

The evolution of Eqs. (13) and (14) is shown as Eqs. (15) and (16):

$$E_T(T)=E_0[1-D(T)] \quad (15)$$

$$v_T^2 = v_0^2[1-D(T)] \quad (16)$$

As for the relationship between damage and temperature, it assumes a rising trend, but it is not unlimited as the temperature increases. The damage approaches 1 gradually after the critical temperature but is no more than 1 in any case. The reason is that the internal structure of the rock is weakened by the expansion and transfixion of micro-cracks and the evaporation of free water is subjected to severe damage after the critical temperature. In this respect, the fitting curve indicates the damage before the critical temperature.

As can be seen, the increased amplitude of thermal damage under an axial pressure of 20 MPa is greater than that described by the longitudinal wave velocity, especially when the temperature rises to 200 °C. In addition, the thermal damage described at the axial pressure of 20 MPa is greater than that described at the longitudinal wave velocity due to the weakening of axial pressure on the internal structure of the granite. Finally, the weakening effects of the axial pressure on the internal structure of the rock are greater with increasing temperature. That is to say, the effects of the dynamic mechanical parameters are greater as the temperature increases.

In Fig. 10, TDD and TTD refer to the dynamic damage under axial pressure of 20 MPa and the thermal

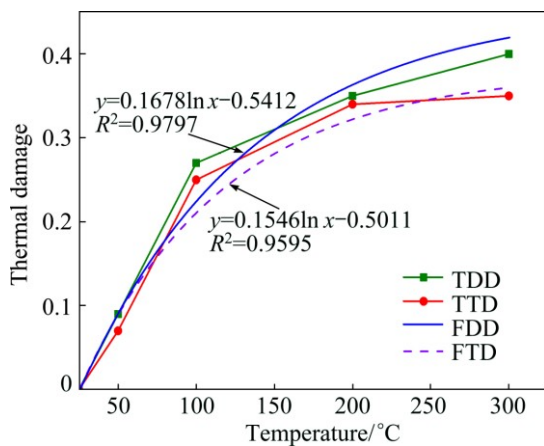


Fig. 10 Relationship between thermal damage and temperature of rock

damage represented by wave velocity, respectively. FDD represents the fitted curve of dynamic damage under axial pressure of 20 MPa, and FTD is the fitted curve of thermal damage represented by wave velocity.

4 Discussion

The experimental results show some discrepancies because of device errors, human errors, differences between samples and the effects of temperature on the incident bar and transmission bar. Nevertheless, these discrepancies, to a certain extent, do not affect the change rules of the physical and mechanical characteristics with the increase of temperature. Thus, the averages of the parameters, excepting the large scatters, were used to analyze the change rules. By introducing the relative amplitude growth (reduction), the relationships among longitudinal wave velocity, peak stress, peak strain and temperature were analyzed. The relative amplitude growth (reduction), even if the temperature gradient is greater, may be smaller. For example, at temperatures from 50 to 100 °C, the relative amplitude reduction of peak stress is 15.98%, while it is only 6.67% at temperatures between 100 and 200 °C. The two main reasons are the differences of main influencing factors on each temperature stage and the non-homogeneous material of rock. In detail, compared with temperatures between 50 and 100 °C, the degradation function of the expansion and transfixion of newborn cracks is less than that of primary cracks. Furthermore, the effects of temperature on the longitudinal wave velocity are greater than on the dynamic mechanical properties. This is because the longitudinal wave velocity is measured before compressing, in which condition the free water evaporates and newborn cracks expand and transfix as the temperature increases, while the dynamic mechanical properties are measured after compressing, in which condition the cracks close under the axial pressure with the increase of temperature. The internal structure of the rocks can be identified by scanning electron microscopy [21], as shown in Fig. 11. It is worth noting that a number of fragments were examined when using the scanning electron microscope, and a typical one was chosen. Rock is a kind of inhomogeneous material and contains some primary cracks and pores. As shown in Figs. 11(a, a'), there is no large crack, but micro-cracks emerge when the fragment is magnified. Moreover, the joint fissures show clearly and the cracks are in the form of straight lines. For a rock under room temperature, although there are primary cracks and pores, the ability to resist damage is high. It is to say, the rock sample has fine mechanical properties. When the rock sample suffers pressure which is high enough, the rock will break along

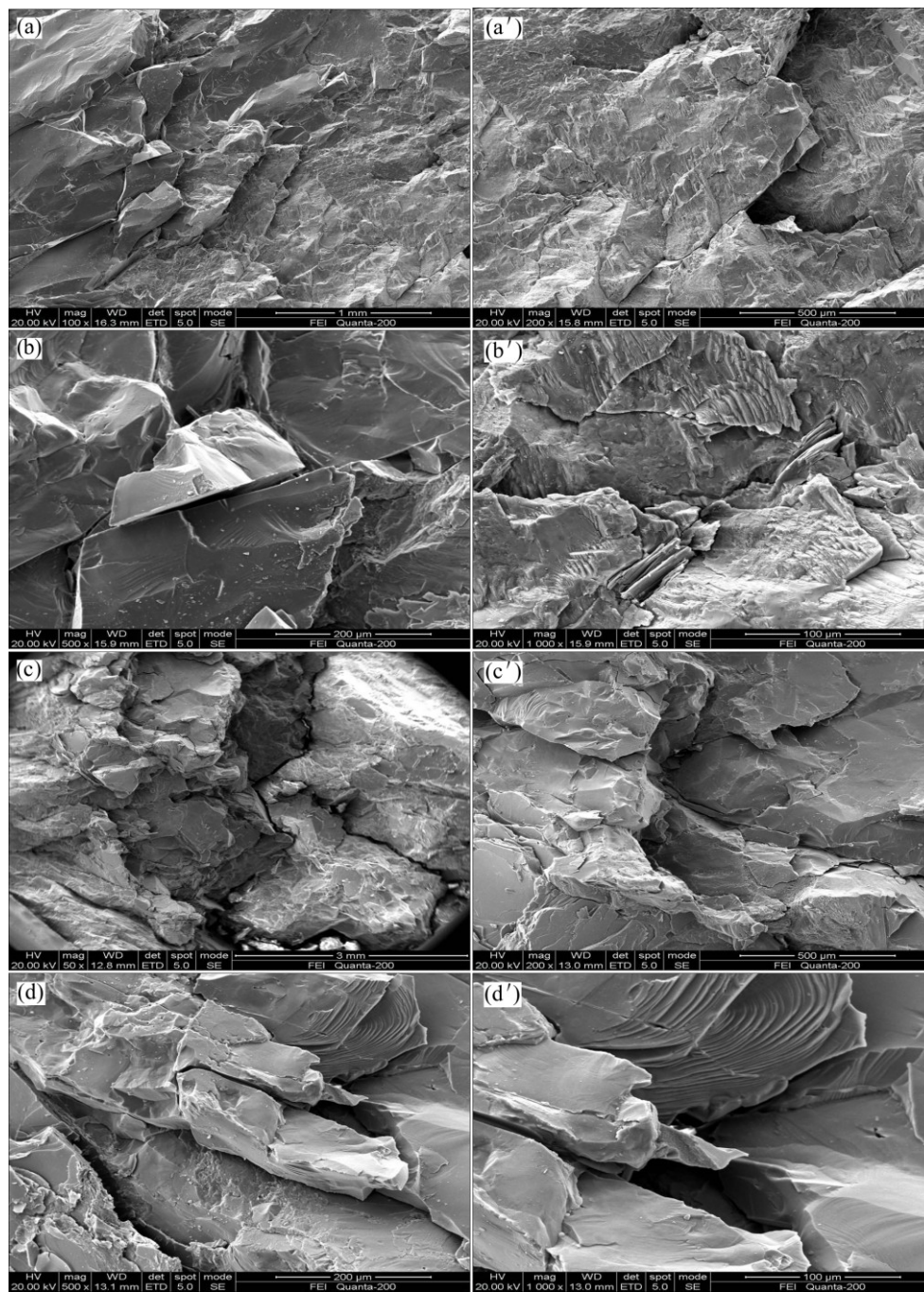


Fig. 11 SEM images of granite fragments after dynamic damage at different temperatures: (a, a') Room temperature; (b, b') 100 °C; (c, c') 200 °C; (d, d') 300 °C

the weak cracks. When heated to 100 °C, the number of cracks increases slightly, and the flake dissection and parallel stripy indentation become gradually apparent, as shown in Figs. 11(b, b'). Under that condition, the free water of primary cracks and pores evaporates, and then the primary cracks and pores emerge gradually. When subjected to axial pressure, some primary cracks and pores close, but the number of visible cracks and pores under electron microscopy are more than that of rock at room temperature. As the temperature rises to 200 °C,

several cracks transfix and rock fragments appear columnar peeling patches as observed in Figs. 11(c, c'). Although, the axial pressure and the expansion of mineral compositions inhabit some cracks and fissures to expand, high temperature leads to further expansion of cracks and creation of fissures. When the temperature continues to increase, reaching 300 °C, the rock fragments display small tattered flakes, presenting bulks peeling along the beddings, which have a terrace shape. Furthermore, the number of cracks varies a little, the

crack sizes increase to some extent and major fractures gradually appear as seen in Figs. 11(d, d'). Under a high temperature, the thermal stress is large, the separation of combined water and the expansion of rock compositions lead to a large change of the structure of rock. Also, some cracks and fissures will be inhabited to expand by the axial pressure and the expansion of mineral compositions, but the effects are small. The free water evaporates with the rising temperature, thus the number of micro-cracks increases accordingly. Owing to the differences of thermal expansion coefficients of crystalline grains, thermal expansion also leads to the increase of micro-cracks and fissures. When the temperature continues to increase, the thermal stress occurs obviously and leads to further expansion of cracks and creation of fissures. These variations of the internal structure of the rocks to a certain extent verify the change rules of longitudinal wave velocity, peak stress and peak strain as the temperature increases. It is also reasonable to say that the variations of longitudinal wave velocity, peak stress, peak strain and elastic modulus are all related to the changes of micro-cracks with increasing temperature.

In addition, some things should be noticed that there are consanguineous interaction among impact loading, axial pressure and temperature under the whole process of experiment. When temperature is below 100 °C, the free water evaporates drastically, the density decreases gradually and temperature accelerates cracks extending. Surely, the axial pressure inhibits the cracks extending. But, as the temperature continues to increase, reaching 300 °C, there are some added reasons except for the above-mentioned. The rock shows a phenomenon of softening with the increasing temperature. Therefore, the inhibition of axial pressure on cracks extending shows more evidently. At that stage, compared with the rock under temperature below 100 °C, the new-born cracks are less and more cracks close under the effect of axial pressure due to softening phenomenon. Thus, when suffered a dynamical load, the dynamical mechanical properties of rock under axial pressure and temperature below 100 °C change more obviously than those of rock above 100 °C.

5 Conclusions

1) The uniaxial compressive strength of granite under an axial pressure of 20 MPa exhibits a declining trend which drops rapidly before 100 °C and presents a non-linear change with the increase of temperature.

2) The longitudinal wave velocity of the rock exhibits a highly sensitive relationship with the temperature increase, falling rapidly before its drops slowly. Moreover, the effects of temperature on peak

stress and peak strain are greater than those on longitudinal wave velocity, which indicates that the effect of temperature on the mechanical properties is greater than on the physical properties.

3) Due to the differences in the degree of influence of the effect of temperature at each stage, the effects of temperature on longitudinal wave velocity, peak stress and peak strain show a non-linear variation. And the relative amplitude growth (reduction), even if the temperature gradient is larger, may be smaller.

4) The thermal damage under an axial pressure of 20 MPa is greater than that described at the longitudinal wave velocity, and becomes more and more obvious with the increase of temperature. Besides, the fitted line can describe the thermal damage before the critical temperature, as well as present a limited increase approaching 1 infinitely. Further, the internal structure of the rock alters greatly as the temperature increases and the changes of longitudinal wave velocity, peak stress, peak strain and elastic modulus are all related to temperature.

References

- [1] LI Xi-bing, ZUO Yu-jun, WANG Wei-hua, MA Chun-de, ZHOU Zi-long. Constitutive model of rock under static–dynamic coupling loading and experimental investigation [J]. Transactions of Nonferrous Metals Society of China, 2006, 16(3): 714–722.
- [2] LI Xi-bing, YAO Jin-rui, GONG Feng-qiang. Dynamic problems in deep exploitation of hard rock metal mines [J]. The Chinese Journal of Nonferrous Metals, 2011, 21(10): 2551–2563. (in Chinese)
- [3] HONG liang, LI Xi-bing, LIU Xi-ling, ZHOU Zi-long, YE Zhou-yuan, YIN Tu-bing. Stress uniformity process of specimens in SHPB test under different loading conditions of rectangular and half-sine input waves [J]. Transactions of Nonferrous Metals Society of China, 2008, 18(2): 450–456.
- [4] DU Kun, LI Xi-bing, LI Di-yuan, WENG Lei. Failure properties of rocks in true triaxial unloading compressive test [J]. Transactions of Nonferrous Metals Society of China, 2015, 25(2): 571–581.
- [5] DONG Long-jun, LI Xi-bing, PENG Kang. Prediction of rockburst classification using random forest [J]. Transactions of Nonferrous Metals Society of China, 2013, 23(2): 472–477.
- [6] YIN Zhi-qiang, LI Xi-bing, JIN Jie-fang, HE Xian-qun, DU Kun. Failure characteristics of high stress rock induced by impact disturbance under confining pressure unloading [J]. Transactions of Nonferrous Metals Society of China, 2012, 22(1): 175–184.
- [7] TIAN H, ZIEGLER M, KEMPKA T. Physical and mechanical behavior of clay stone exposed to temperatures up to 1000 °C [J]. International Journal of Rock Mechanics and Mining Sciences, 2014, 70(5): 144–153.
- [8] LIU Shi, XU Jing-yu. Mechanical properties of Qinling biotite granite after high temperature treatment [J]. International Journal of Rock Mechanics and Mining Sciences, 2014, 71(8): 188–193.
- [9] LIU Shi, XU Jing-yu. An experimental study on the physico-mechanical properties of two post-high-temperature rocks [J]. Engineering Geology, 2015, 185(12): 63–70.
- [10] YANG Sheng-qi, JING Hong-wen, HUANG Yan-hua, RANJITH P G, JIAO Yu-yong. Fracture mechanical behavior of red sandstone containing a single fissure and two parallel fissures after exposure to different high temperature treatments [J]. Journal of Structural

- Geology, 2014, 69(1): 245–264.
- [11] XU Xiao-li, GAO Feng, SHEN Xiao-ming, XIE He-ping. Mechanical characteristics and microcosmic mechanisms of granite under temperature loads [J]. Journal of China University of Mining and Technology, 2008, 18(3): 413–417.
- [12] XU Xiao-li, KANG Zong-xin, JI Ming, GE Wen-xuan, CHEN Jing. Research of microcosmic mechanism of brittle-plastic transition for granite under high temperature [J]. Procedia Earth and Planetary Science, 2009, 1(1): 432–437.
- [13] SHAO S S, RANJITH P G, WASANTHA P L P, CHEN B K. Experimental and numerical studies on the mechanical behaviour of Australian Strathbogie granite at high temperatures: An application to geothermal energy [J]. Geothermics, 2015, 54(1): 96–108.
- [14] WU Gang, WANG De-yong, ZHAI Song-tao, LI Yu-shou, CHEN Jun. Test research on mechanical properties of marble under high temperature [J]. Chinese Journal of Rock Mechanics and Engineering, 2012, 31(6): 1237–1244. (in Chinese)
- [15] ZHAO Yang-sheng, FENG Zi-jun, XI Bao-ping, WAN Zhi-jun, YANG Dong, LIANG Wei-guo. Deformation and instability failure of borehole at high temperature and high pressure in hot dry rock exploitation [J]. Renewable Energy, 2015, 77(12): 159–165.
- [16] LIU Shi, XU Jing-yu. Study on dynamic characteristics of marble under impact loading and high temperature [J]. International Journal of Rock Mechanics and Mining Sciences, 2013, 62(5): 51–58.
- [17] FUNATSU T, SETO M, SHIMADA H, MATSUI K, KURUPPU M. Combined effects of increasing temperature and confining pressure on the fracture toughness of clay bearing rocks [J]. International Journal of Rock Mechanics and Mining Sciences, 2004, 41(6): 927–938.
- [18] BIENIAWSKI Z T, BEMEDE M J. Suggested methods for determining the uniaxial compressive strength and deformability of rock materials: Part 1. Suggested method for determining deformability of rock materials in uniaxial compression [J]. International Journal of Rock Mechanics and Mining Sciences and Geomechanics Abstracts, 1979, 16(2): 138–140.
- [19] XU Xi-chang. Study on the characteristics of thermal damage for granite [J]. Chinese Journal of Geotechnical Engineering, 2003, 24(S2): s188–s191. (in Chinese)
- [20] ZHANG Zhi-zhen, GAO Feng, XU Xiao-li. Experimental study of temperature effect of mechanical properties of granite [J]. Chinese Journal of Geotechnical Engineering, 2011, 32(8): 2346–2352. (in Chinese)
- [21] ZHANG Zhi-zhen, GAO Feng, LIU Zhi-jun. Research on rock burst proneness and its microcosmic mechanism of granite considering temperature effects [J]. Chinese Journal of Rock Mechanics and Engineering, 2010, 29(8): 1591–1602. (in Chinese)

温度和轴压对花岗岩动态力学性能的影响

尹土兵, 舒荣华, 李夕兵, 王品, 董陇军

中南大学 资源与安全工程学院, 长沙 410083

摘要: 为了得到高温高应力下岩石的动态力学性能, 对其进行冲击加载实验。对 SHPB 实验系统进行改进, 使该系统能够实现温度与轴压共同作用下的冲击加载实验。采用扫描电子显微镜观察花岗岩碎片的内部结构特征。研究表明: 花岗岩的纵波波速随温度的升高呈下降趋势, 先快速后缓慢下降; 花岗岩的单轴动态抗压强度随温度的升高呈下降趋势, 其值在 25~100 °C 比在 100~300 °C 时下降得更加明显; 峰值应变则随温度的升高而逐渐增大, 同样以 100 °C 为分界点, 先快速后缓慢增加; 随着温度的增加, 花岗岩内部发生了巨大的变化, 如原生裂纹和新生裂纹的扩展和贯通。另外, 轴压下的热损伤比以波速表征的热损伤大, 特别是随着温度的增加, 这种现象更加明显。

关键词: 岩石冲击动力学; 分离式霍普金森压杆; 温压耦合; 动态力学特性

(Edited by Wei-ping CHEN)